TE
5092
.M8A3
no.68-1

MISSOURI COOPERATIVE HIGHWAY RESEARCH PROGRAM
REPORT **68-1**

BUREAU OF PUBLIC ROADS
RECEIVED
JUN 10 1969
LIBRARY

"SHEAR CONNECTIONS IN HAUNCHED COMPOSITE MEMBERS"

Property of
MoDOT TRANSPORTATION LIBRARY

MISSOURI STATE HIGHWAY DEPARTMENT
UNIVERSITY OF MISSOURI - COLUMBIA
BUREAU OF PUBLIC ROADS

TE
5092
.M8A3
no.68-1

PB 182 116

"SHEAR CONNECTIONS IN HAUNCHED COMPOSITE MEMBERS"

Prepared for

MISSOURI STATE HIGHWAY DEPARTMENT

by

JAMES W. BALDWIN, JR.

and

SANKAR C. DAS

DEPARTMENT OF CIVIL ENGINEERING

UNIVERSITY OF MISSOURI

COLUMBIA, MISSOURI

BUREAU OF PUBLIC ROADS
RECEIVED
JUN 10 1969
LIBRARY

in cooperation with

U.S. DEPARTMENT OF TRANSPORTATION

FEDERAL HIGHWAY ADMINISTRATION

BUREAU OF PUBLIC ROADS

The opinions, findings, and conclusions expressed in this publication are not necessarily those of the Bureau of Public Roads.

TABLE OF CONTENTS

CHAPTER		PAGE
I.	INTRODUCTION	1
	1.1 General	1
	1.2 Slab with Haunches	2
	1.3 Object and Scope	5
II.	EXPERIMENTAL INVESTIGATION	7
	2.1 Description of Specimens and Apparatus	7
	2.1.1 Pushout Specimens	7
	2.1.2 Materials	7
	2.1.3 Preparation of Specimens	7
	2.1.4 Loading Apparatus and Instrumentation.	9
	2.2 Test Procedure	9
	2.3 Experimental Results	10
	2.3.1 Pushout	10
	2.3.2 Cylinders	10
III.	THEORETICAL ANALYSIS	14
	3.1 Elastic Analysis	14
	3.1.1 Introduction	14
	3.1.2 Application of the Elastic Equations	16
	3.1.3 Location of the Principal Stress Trajectories	19
	3.2 Ultimate Strength Analysis at Incipient Failure	22
	3.2.1 Redistribution of Loading after the Tensile Crack	22

CHAPTER PAGE

3.2.2 Assumption and Analysis 22

3.2.3 Comparison of Experiment and Theory . 26

3.2.4 Analysis of the Load per Shear Connection with More than One Line of Studs in the Zone of Influence . . 28

IV. DESIGN IMPLICATIONS 36

4.1 Introduction 36

4.2 Relationship between the Width of the Slab and the Total Force at the Section of Shear Connectors 37

4.3 Relationship between the Spacing of Studs and the Strength of the Shear Connection . . 39

V. CONCLUSIONS 42

SELECTED REFERENCES 44

LIST OF FIGURES

FIGURE		PAGE
1.	Details of Haunched Pushout as Investigated by Buttry	3
2.	Comparison of the Haunched Section with the Narrow Rectangular Slab	4
3.	Details of Pushout Specimens	8
4.	Specimen N6B4HS-1 after Failure	12
5.	Specimen N6B4HS-2 after Failure	12
6.	Specimen N6B4HS-3 after Failure	13
7.	Specimen N6B4HS-4 after Failure	13
8.	Concentrated Force, P, Acting at a Point Internal to a Half Plane	15
9.	Linear Distribution of Load along the Length of the Stud	17
10.	Assumed Force Distribution in Slab	17
11.	Division of Vertical Load Distribution in the Slab into a Finite Number of Concentrated Loads	18
12.	Maximum Principal Stress Trajectories	20
13.	Maximum Shear Stress Trajectories	21
14.	Redistribution of Loading after the Tensile Crack	23
15.	Assumed Failure Surface, AB	24
16.	Haunched Section	30
17.	Assumed Failure Surfaces, A_1B_1, A_2B_2, and A_3B_3	33
18.	Strength of Shear Connection vs. Width of Slab	38
19.	Dimensionless Plot of Shear Connection Strength vs. Stud Spacing	40

LIST OF TABLES

TABLE		PAGE
I.	Results of Pushout and Cylinder Tests	11
II.	Values of θ and n	27
III.	Comparison of Theoretical Load per Connector with Expt. Results from Pushout Tests	29
IV.	Comparison of Theoretical Load per Connector with Expt. Results of the Haunched Sections Taken from Buttry's Work	31
V.	Comparison of Theoretical Load per Connector with Expt. Results of the Haunched Section Taken from Sweeney's Work	32

CHAPTER I

INTRODUCTION

1.1 GENERAL

Composite construction in steel and concrete may be traced to the patent "Composite Beam Construction" issued to J. Kahn in 1926 and to the early studies of R. A. Caughey (1)* published in 1929. Several highway bridges of composite construction were built in the nineteen thirties and early nineteen forties.

The first specification (2) for design of composite highway bridges was published by the American Association of State Highway Officials (AASHO) in 1944, which merely outlined principles and left the method and application to the discretion of the designer. Systematic research studies and the vast amount of experience accumulated in the following decade, indicated a need for more detailed provisions. Accordingly the AASHO published in 1957 a new, substantially expanded version of the specification for design of composite bridges (3).

In bridge construction, the concrete slab sometimes does not rest directly on the top flange of the I-beam. Instead a concrete haunch or fillet is inserted between the slab proper and the beam. By varying the depth of this haunch it is possible to compensate for the dead load deflection and to allow for vertical curves or cross-slopes in the road surface.

*Numbers in parentheses refer to entries in the list of references

1.2 SLAB WITH HAUNCHES

The use of shear-connectors in conjunction with haunched slabs requires some special considerations. The use of a relatively high narrow haunch may result in a very high stress in the concrete around the shear connectors. Sweeney (4), in his investigation of composite-beam stringers, observed premature failures resulting from the haunch. Since then it has been a concern to know the actual behavior of haunched composite members.

Buttry (5) made some pilot studies with pushout tests (Fig. 1) and in some cases observed reductions of 25 percent in the capacity of the shear connection.

In a haunched pushout as in a beam, the capacity of the shear connection is dependent on the rather complex geometry of the section. In an attempt to find the effect of the haunch on the load-carrying capacity of the shear connector, great difficulties were encountered with this complex geometry.

The additional variables introduced by the geometry of the haunched section, Fig. 2, are:

w_1 - lower width of the haunch

w_2 - upper width of the haunch

h - height of the haunch

t - thickness of the concrete slab

A very large number of specimens would be required to develop an empirical relation including all these variables in addition

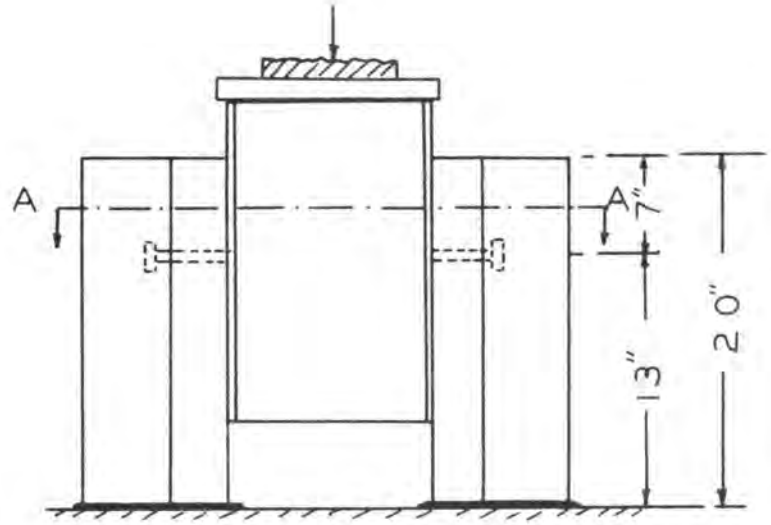

ELEVATION

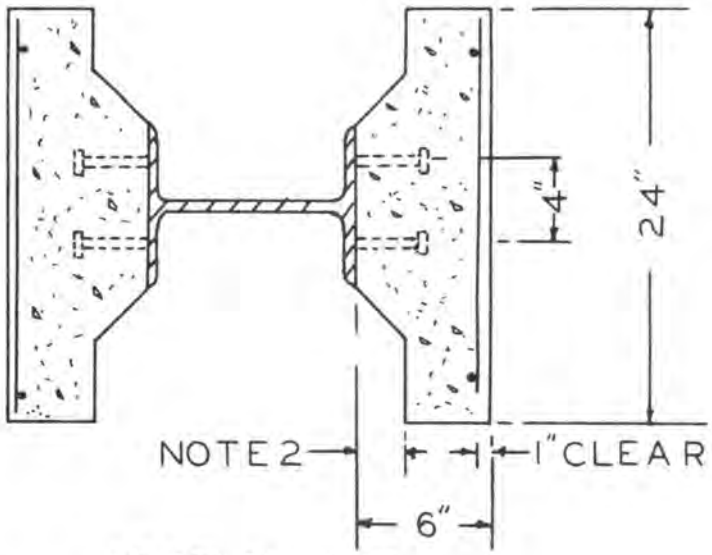

SECTION A-A

NOTES:

1- ALL BEAMS WERE 8WF48
2- HAUNCHES WERE EITHER 1.5" OR 3"

FIG. 1 DETAILS OF HAUNCHED PUSHOUT AS INVESTIGATED BY BUTTRY

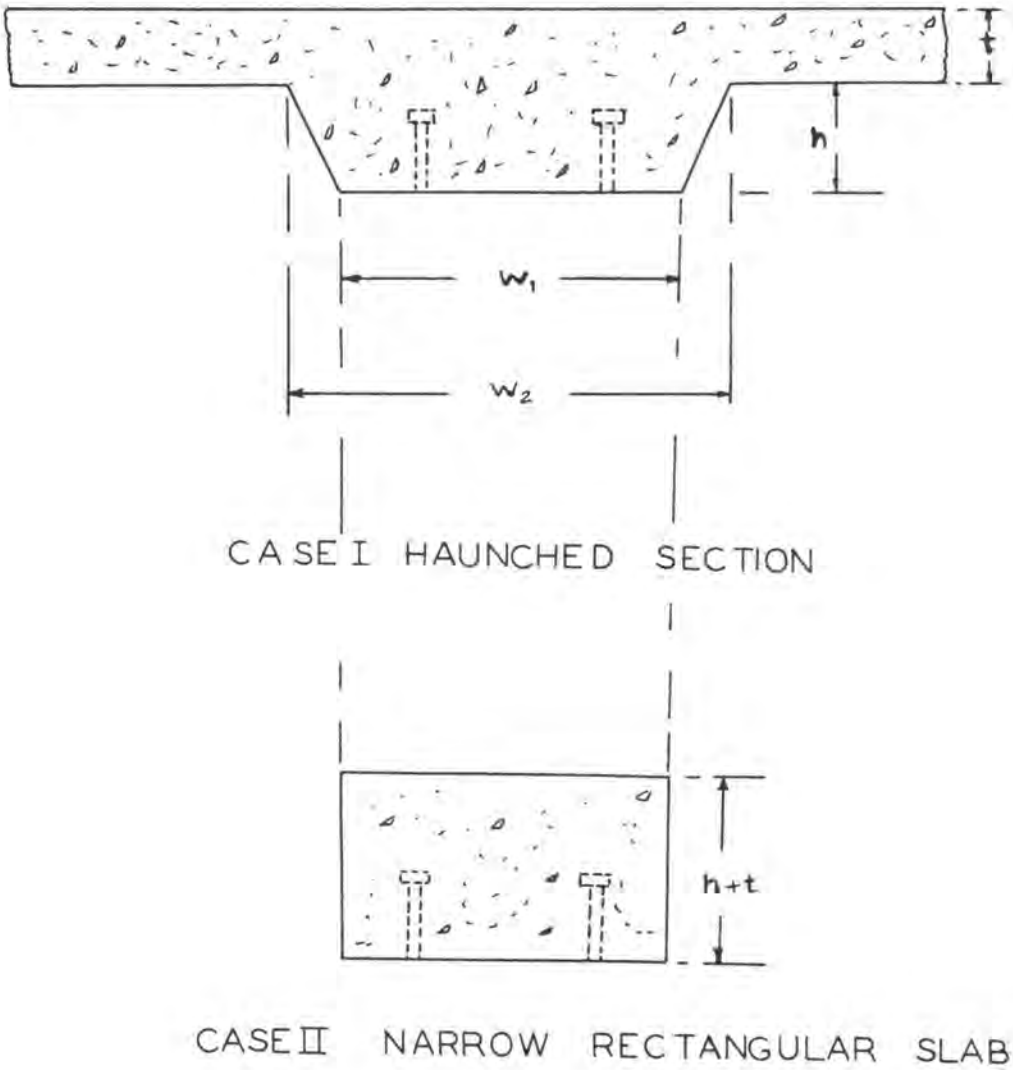

FIG. 2 COMPARISON OF THE HAUNCHED SECTION WITH THE NARROW RECTANGULAR SLAB

to the variables governing the strength of shear connectors in a solid slab. The problem was simplified by assuming that the strength of a shear connection in the narrow rectangular slab with width w_1 (Fig. 2) is a conservative estimate of the strength of a shear connection in the haunched section.

In cases where the sides of the haunch are steep and the shear connectors do not extend through the haunch, this assumption is only slightly conservative. In cases where the shear connectors extend into the main slab, this assumption is considerably more conservative. Thus in the present work, the narrow rectangular slab was taken as the basis of analysis.

1.3 OBJECT AND SCOPE

The object of this study was to develop an expression to predict a lower bound for the capacity of stud shear connectors in composite beams with haunched slabs.

This report covers a theoretical analysis as well as test results of eight pushout specimens. The analysis consists of two parts, one an elastic analysis of the uncracked slab and the other an ultimate strength analysis at incipient failure.

The experimental results of the pushouts were used to determine empirical values for coefficients in the analysis.

The symbols adopted for use in the report are arranged alphabetically below and also are defined where they first appear.

D - Diameter of stud

E_c - modulus of elasticity of concrete

E_s - modulus of elasticity of steel

f'_c - compressive strength of concrete

f'_s - shear strength of steel

h - height of the haunch

L - length of stud

M_P - plastic moment capacity of the stud

N - total number of studs at the section of a shear connection

n - empirically determined exponent

P - total force at the section of a shear connection

$\hat{P}$ - total force at the section of a shear connection with more than one line of studs in the zone of influence

Q - load per stud

Q_s - ultimate shearing strength of stud

s - failure length

$\hat{s}$ - stud spacing

t - thickness of the concrete slab

w - width of the slab

w_1 - lower width of the haunch

w_2 - upper width of the haunch

$w_{av.}$ - average width of the haunch

$\sigma 1$ - maximum principal stress

$\sigma 2$ - minimum principal stress

τ - maximum shear stress

$\tau_{max.}$ - shearing strength of concrete

ν - Poisson ratio

CHAPTER II

EXPERIMENTAL INVESTIGATION

2.1 DESCRIPTION OF SPECIMENS AND APPARATUS

2.1.1 Pushout Specimens. The pushout specimens used are shown in detail in Fig. 3. Specimens consisted of an 8WF48 beam section and two concrete slabs 20x8x6 inches. There were two studs on each flange of the steel beam.

Four specimens were fabricated with ½x4-inch studs and four specimens were fabricated with 3/4x4-inch studs.

2.1.2 Materials. The concrete for the slabs of the pushout specimens consisted of normal-weight aggregate and type I Portland cement. The coarse aggregate was well graded crushed limestone with a maximum size of 3/4 inches and the fine aggregate was Missouri River sand. Typical mix proportions were 1:1.94:3.27 by weight with a water-cement ratio of 5.0 gallons per sack. This mix conformed with the class B-1 mix required by the State Highway Commission of Missouri for bridge construction. The concrete was obtained from a local ready-mix plant.

2.1.3 Preparation of Specimens. Headed studs were welded by a commercial end welding process to the 8WF48, A-36 steel beam stub.

The slabs were cast on edge and the concrete was carefully vibrated to eliminate air voids in the vicinity of the studs. The concrete was cured in the laboratory with wet burlap and a polyethylene covering for 28 days. Four pushout specimens and

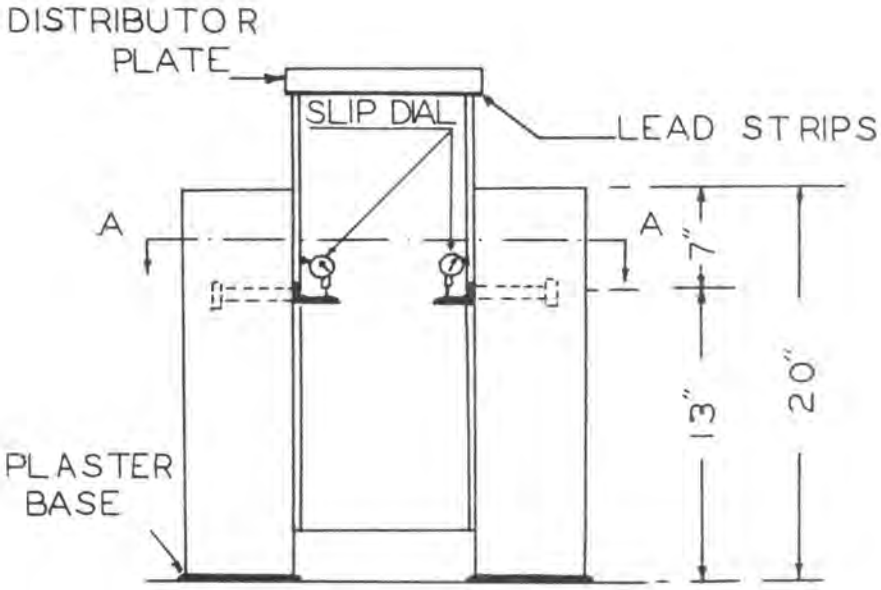

ELEVATION

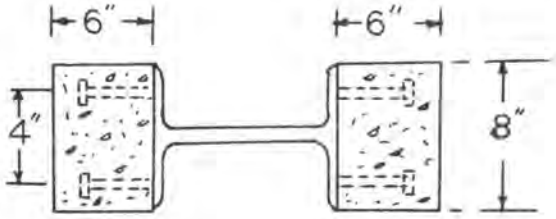

SECTION A-A

FIG. 3 DETAILS OF PUSHOUT SPECIMENS

six 6x12-inch cylinders were cast with each batch and cured under the same conditions. At the end of 28 days the pushout specimens and the cylinders were allowed to air dry.

2.1.4 Loading Apparatus and Instrumentation. The pushout specimens were tested in a 300,000 lb. capacity hydraulic testing machine. Load was applied to the end of the steel beam section through a spherical block and a steel distributing plate. Slip between the slabs and the beam section were measured with four 0.001-inch dial indicators mounted at the locations shown in Fig. 3. Each dial was rigidly attached to the appropriate steel beam flange with the dial stem bearing on a bracket cemented to the concrete slab. The dials and brackets were placed directly opposite the shear connectors.

2.2 TEST PROCEDURE

Pushout specimens were preloaded up to 15,000 lbs. to check the dial indicators. The loading procedure for all pushouts was to load the specimen in cycles with each successive cycle having a higher peak load. A typical series of loading cycles was 0, 5, 10, 5, 0, 5, 10, 15, 10, 5, 0, 10, 15, 20, 15, 10, 0, 10, 20, 25 . . . where each number is the magnitude of the load in kips at which the dial indicators were read.

The load was held constant at each level while all dial indicator readings were recorded. As the specimen approached failure, the dials indicated that the slip was increasing even though the load was held constant. Under this condition the dials were read at the instant the testing machine operator reported the

load had reached the desired value.

2.3 EXPERIMENTAL RESULTS

2.3.1 Pushout. The results of the pushout tests are summarized in Table I. In each case the load per stud represents the total load applied divided by the number of connectors on the specimen.

Pushout specimens with ½-inch diameter studs failed by shearing of the studs. Pushout specimens with 3/4-inch diameter studs first developed "principle tensile cracks" in both the slabs. These tensile cracks started from the foot of the studs and progressed through the structure of the slabs. After development of the tensile cracks, there was a redistribution of stresses in the slabs and the final failure developed along shear surfaces as shown in Figs. 4 through 7.

2.3.2 Cylinders. The testing machine used for the pushouts was also used to test six cylinders in compression for each series of pushout specimens. Three cylinders were tested to failure according to ASTM C 39-66, to determine the compressive strength of concrete. The remaining three cylinders were then tested according to ASTM C 469-65, to determine the modulus of elasticity of the concrete. An average of the three ultimate loads was used to determine the compressive strength and the modulus of elasticity was taken to be the average of the three tests. Results of the cylinder tests are given in Table I.

TABLE I

RESULTS OF PUSHOUT AND CYLINDER TESTS

Specimen	Stud diameter (inches)	Stud length (inches)	f'_c (ksi)	E_c (ksi)	Critical Load* Av. slip (inches)	Critical Load* Load/stud (kips)	Ultimate Load Av. slip (inches)	Ultimate Load Load/stud (kips)	Type of failure
N4B4HS-1	.500	4.0	8.28	4.52×10^3	.1056	10.00	-	12.12	Stud
N4B4HS-2	.500	4.0	8.28	4.52×10^3	-	-	.1028	13.12	Stud
N4B4HS-3	.500	4.0	6.861	4.18×10^3	.0688	10.00	-	11.25	Stud
N4B4HS-4	.500	4.0	6.861	4.18×10^3	.0520	12.50	-	12.87	Stud
N6B4HS-1	.750	4.0	8.28	4.52×10^3	-	-	-	18.50	Concrete
N6B4HS-2	.750	4.0	8.28	4.52×10^3	-	-	.0329	23.75	Concrete
N6B4HS-3	.750	4.0	6.861	4.18×10^3	.0175	15.0	.0329	17.13	Concrete
N6B4HS-4	.750	4.0	6.861	4.18×10^3	.0272	15.0	-	20.0	Concrete

*Load at which slip dial would not stabilize and in the case of 3/4-inch dia. studs, this gives the load at which tensile cracks developed.

-Readings were not possible to record.

FIG.4 SPECIMEN N6B4HS-1 AFTER FAILURE

FIG.5 SPECIMEN N6B4HS-2 AFTER FAILURE

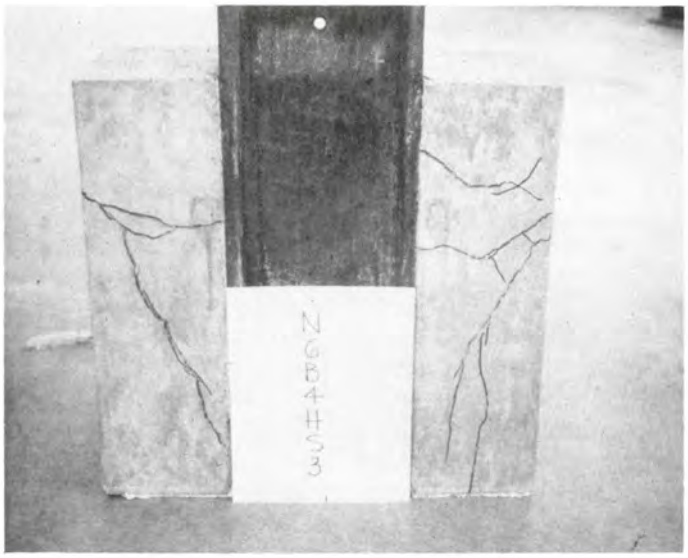

FIG. 6 SPECIMEN N6B4HS-3 AFTER FAILURE

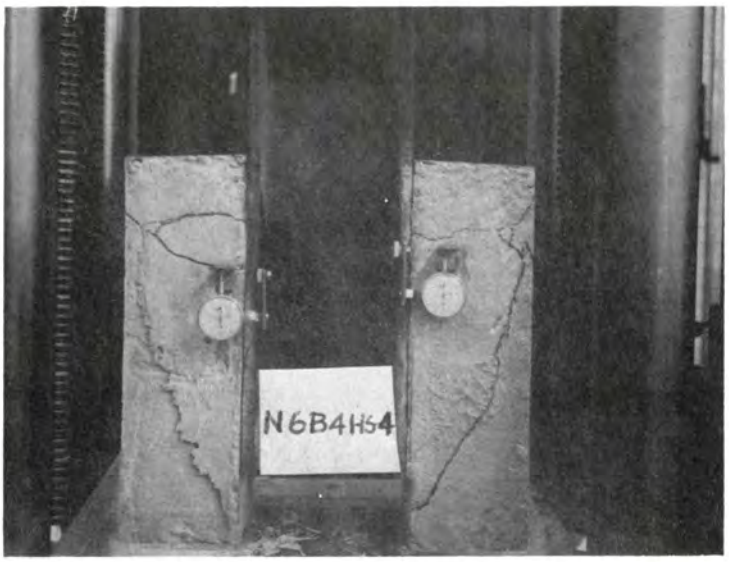

FIG. 7 SPECIMEN N6B4HS-4 AFTER FAILURE

CHAPTER III

THEORETICAL ANALYSIS

3.1 ELASTIC ANALYSIS

3.1.1 Introduction. E. Melan (6) found the plane stress elastic solutions of a concentrated force, acting at a point internal to a half plane. Referring to Fig. 8, the equations for the stresses at any point of the half plane are as follows:

$$\sigma_{x-x} = \frac{P}{2\pi(\kappa+1)}\{(\kappa-1)y\cdot\frac{1}{r_1^2} - 4yx_1^2\cdot\frac{1}{r_1^4} - (\kappa-1)y\cdot\frac{1}{r_2^2}$$

$$- 4y[\kappa x_2^2 - c(\kappa-1)x_2 - 2c^2]\cdot\frac{1}{r_2^4} + 32cyx_2(x_2^2-cx_2)\frac{1}{r_2^6}\} \quad (1)$$

$$\sigma_{y-y} = \frac{P}{2\pi(\kappa+1)}\{-(\kappa+3)y\cdot\frac{1}{r_1^2} + 4yx_1^2\cdot\frac{1}{r_1^4} - (3\kappa+1)y\cdot\frac{1}{r_2^2}$$

$$+ 4y[\kappa x_2^2 - c(\kappa+3)x_2 - 2c^2]\cdot\frac{1}{r_2^4} + 32cyx_2(y^2+cx_2)\cdot\frac{1}{r_2^6}\} \quad (2)$$

$$\tau_{x-y} = \frac{P}{2\pi(\kappa+1)}\{-(\kappa+3)x_1\frac{1}{r_1^2} + 4x_1^3\frac{1}{r_1^4} + \frac{1}{r_2^2}\cdot$$

$$[-x_2(3\kappa+1) + 2c(\kappa-1)] + 4x_2[\kappa x_2(x_2-c) + c(7x_2-6c)]\frac{1}{r_2^4}$$

$$+ 32cx_2^3(c-x_2)\cdot\frac{1}{r_2^6}\} \quad (3)$$

where,

$$x_1 = x-c$$

$$x_2 = x+c$$

$$r_1^2 = x_1^2+y^2$$

$$r_2^2 = x_2^2+y^2$$

$$\kappa = \frac{3-\nu}{1+\nu}$$

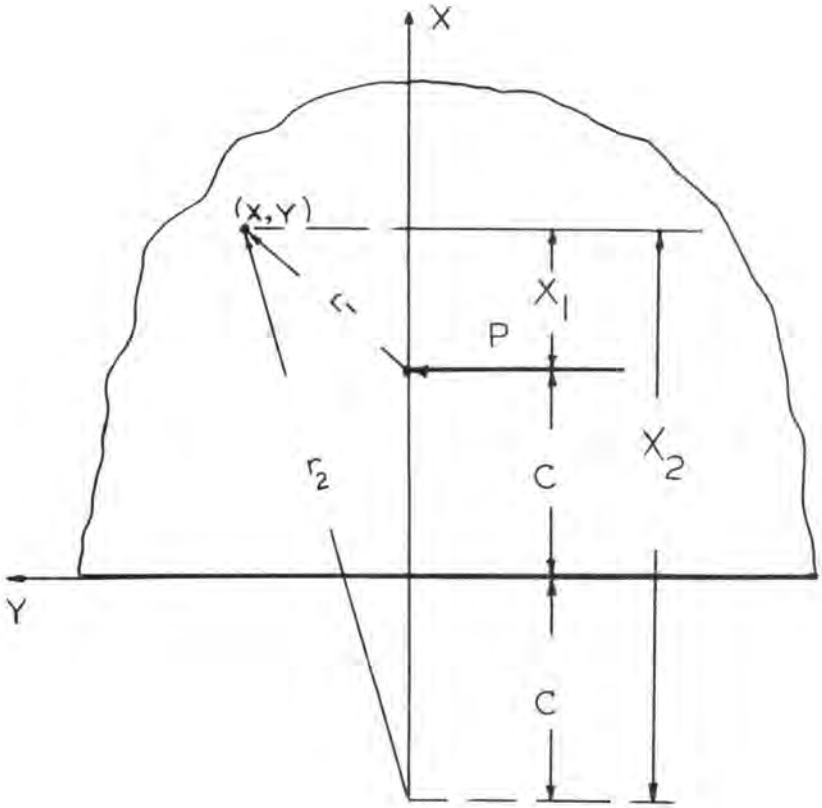

FIG. 8 CONCENTRATED FORCE, P, ACTING AT A POINT INTERNAL TO A HALF PLANE

ν = Poisson ratio

3.1.2 Application of the Elastic Equations. The above elastic solutions of the plane stress problem for a single concentrated load can be applied to the problem of a shear connector in a narrow rectangular slab, Fig. 3. In applying this solution it was necessary to assume that the load from the studs was uniformly distributed across the width of the slab. The exact distribution of force along the length of the stud was not known but the two necessary conditions for this distribution are that, nowhere may the moment in the stud be greater than M_P, the plastic moment capacity of the stud and the integral of this distribution must equal the force in the shear connector.

Various linear distributions along the length of the studs were compared with moment capacities of the studs and the test values of shear connector force. One of the loadings along the length of the stud, which satisfied the above condition, is shown in Fig. 9. The complete assumed distribution of force applied to the slab is shown in Fig.10. Now considering a unit width of the slab, the vertical distribution of load can be divided into a finite number of concentrated loads, Fig. 11. From the principle of superposition, the stress at any point in the slab can be found by summing the values of Eq. 1 through Eq. 3, for each of the finite concentrated loads. Therefore,

$$\sum \sigma_{x-x} = \sigma_{x-x_{P_1}} + \sigma_{x-x_{P_2}} + \sigma_{x-x_{P_3}} + \ldots \tag{4}$$

$$\sum \sigma_{y-y} = \sigma_{y-y_{P_1}} + \sigma_{y-y_{P_2}} + \sigma_{y-y_{P_3}} + \ldots \tag{5}$$

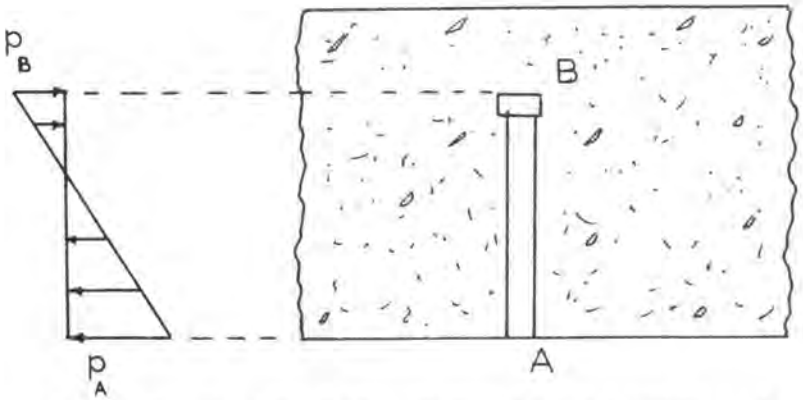

FIG. 9 LINEAR DISTRIBUTION OF LOAD ALONG THE LENGTH OF THE STUD

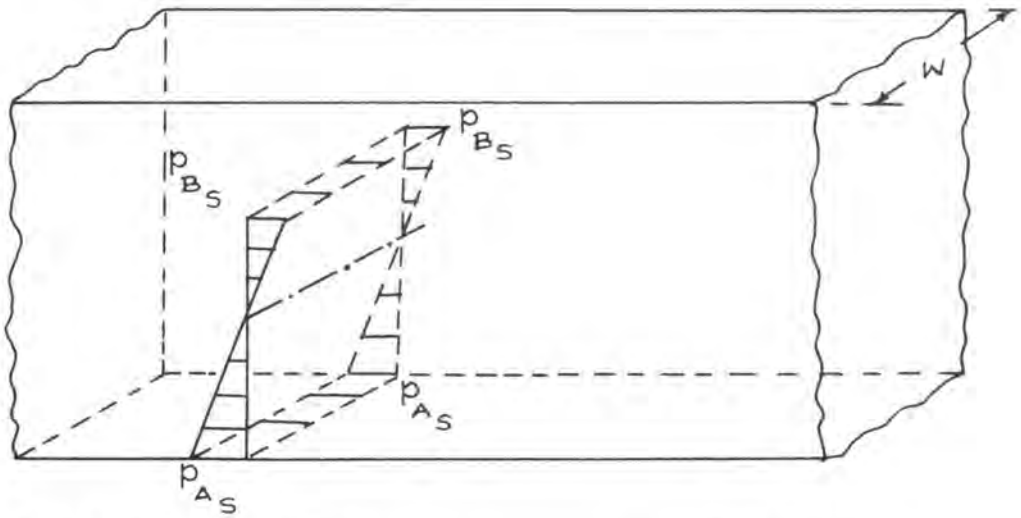

NOTES: $p_{A_S} = \frac{p_A \cdot N}{W}$; $p_{B_S} = \frac{p_B \cdot N}{W}$

WHERE, W = WIDTH OF THE SLAB
N = NO OF STUDS AT THE SECTION, AB

FIG. 10 ASSUMED FORCE DISTRIBUTION IN SLAB

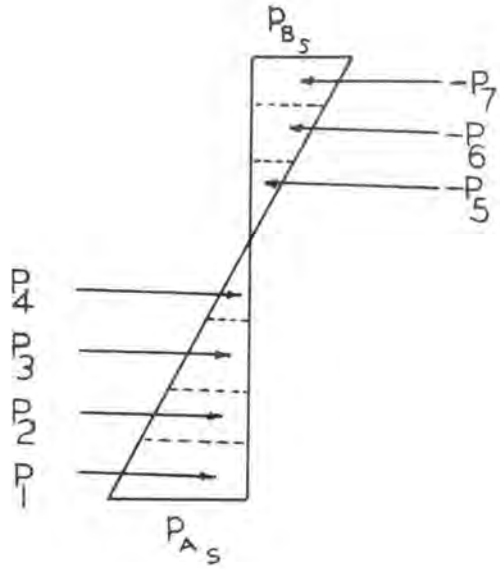

FIG.11 DIVISION OF VERTICAL LOAD DISTRIBUTION IN THE SLAB INTO A FINITE NUMBER OF CONCENTRATED LOADS

$$\sum \tau_{x-y} = \tau_{x-y_{P_1}} + \tau_{x-y_{P_2}} + \tau_{x-y_{P_3}} + \ldots \tag{6}$$

The maximum principal stress,

$$\sigma 1 = \frac{\sum \sigma_{x-x} + \sum \sigma_{y-y}}{2} + \sqrt{\left(\frac{\sum \sigma_{x-x} - \sum \sigma_{y-y}}{2}\right)^2 + (\sum \tau_{x-y})^2} \tag{7}$$

The minimum principal stress,

$$\sigma 2 = \frac{\sum \sigma_{x-x} + \sum \sigma_{y-y}}{2} - \sqrt{\left(\frac{\sum \sigma_{x-x} - \sum \sigma_{y-y}}{2}\right)^2 + (\sum \tau_{x-y})^2} \tag{8}$$

The maximum shear stress,

$$\tau = \sqrt{\left(\frac{\sum \sigma_{x-x} - \sum \sigma_{y-y}}{2}\right)^2 + (\sum \tau_{x-y})^2} \tag{9}$$

The angle between $\sigma 1$ and the y-axis, Fig. 8,

$$\alpha = \tfrac{1}{2}\tan^{-1}\left(\frac{2\sum \tau_{x-y}}{\sum \sigma_{x-x} - \sum \sigma_{y-y}}\right) \tag{10}$$

3.1.3 Location of the Principal Stress Trajectories.

Equations 1 through 10 were applied to a narrow rectangular concrete slab 20x8.5x6 inches with two 7/8x4-inch studs located on the center of the 20-inch dimension of the slab. The shear connector force was 20.5 kips per stud. The stresses at each grid point in the slab were calculated with the help of the computer. Two orthogonal families of curves, one giving the $\sigma 1$ trajectories and the other the surface on which they act are shown in Fig. 12 for the right half of the slab. Maximum shear stress trajectories were also plotted for the left half of the slab and are shown in Fig. 13.

From Fig. 12, one would expect a tensile crack to form along the surface M-M. This is in general agreement with results of the pushout tests, Fig. 4-7, but the formation of this crack does not produce complete failure of the specimen. The load at

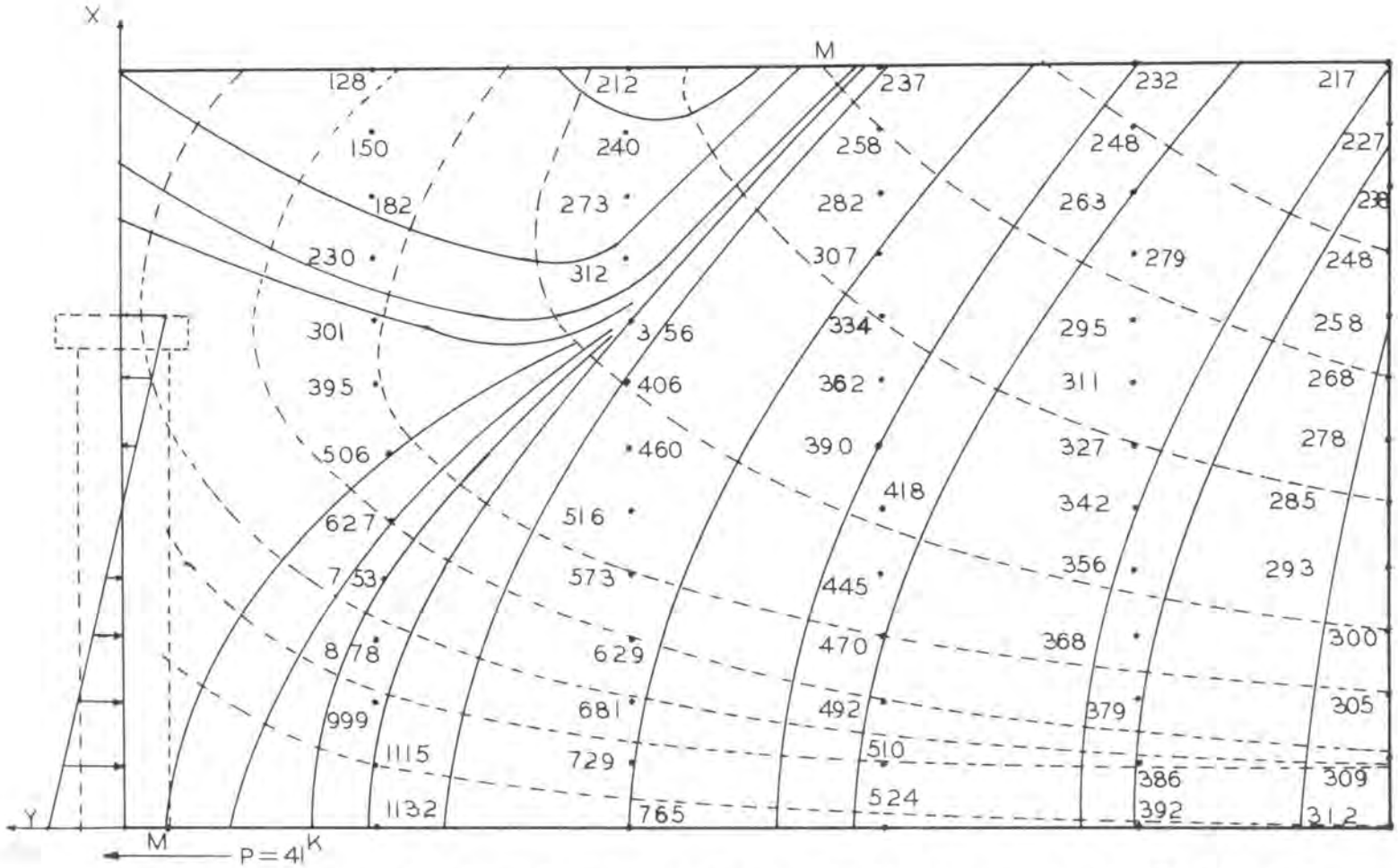

NOTE NUMBERS GIVE THE TENSILE PRINCIPAL STRESSES AT THE POINTS IN PSI.

- - - - - - - - - - TENSILE TRAJECTORIES

———————— TENSILE TRAJECTORY SURFACES

FIG. 12 MAXIMUM PRINCIPAL STRESS TRAJECTORIES

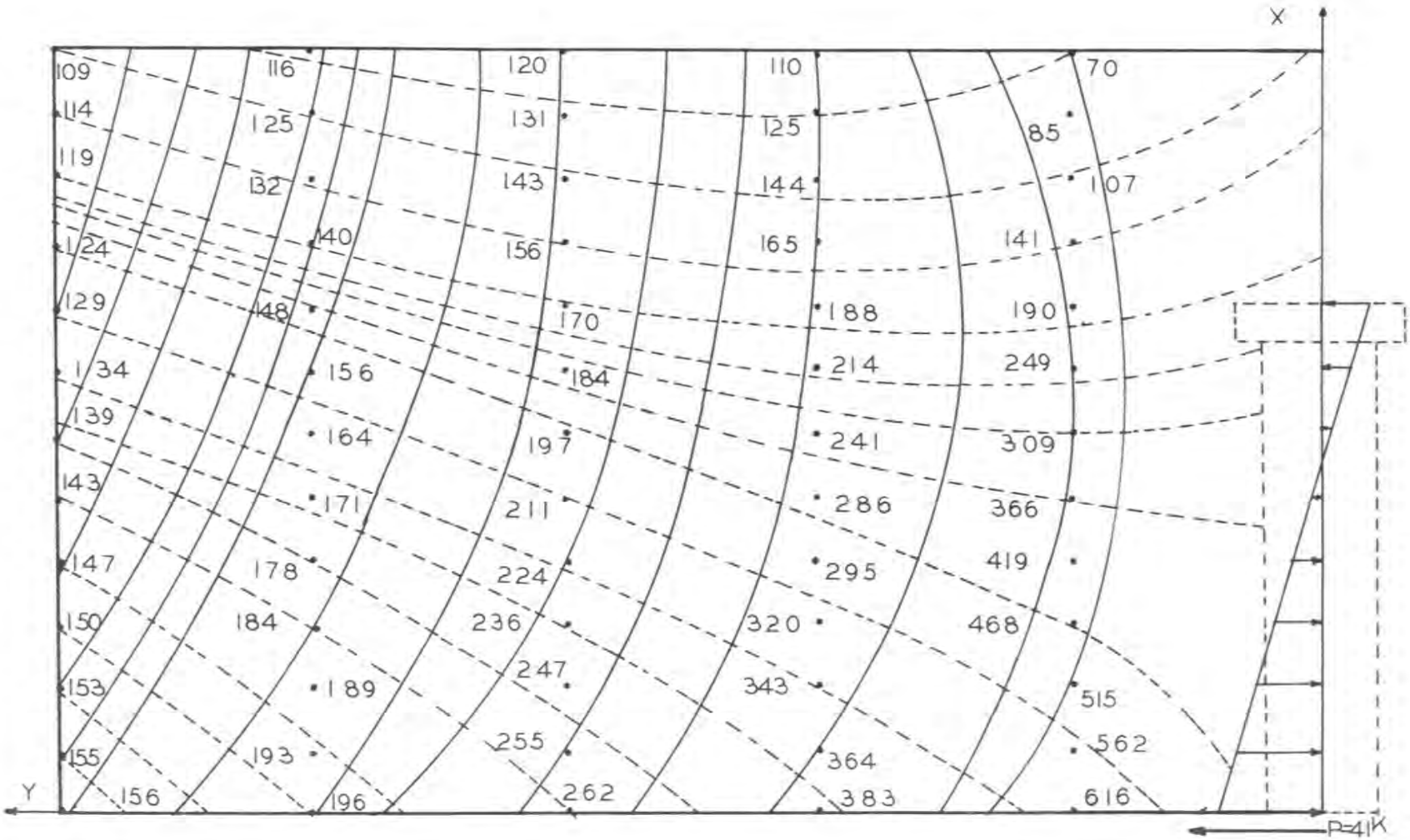

NOTE: NUMBERS GIVE THE MAXIMUM SHEAR STRESSES AT THE POINTS IN P S I.

FIG.13 MAXIMUM SHEAR STRESS TRAJECTORIES

which the tensile crack formed was about 80 percent of the ultimate load, Table I. The elastic analysis of the uncracked slab also indicates that the shear stresses in the slab are low as is shown in Fig. 13.

Since stress strain relations for concrete are non-linear at high stresses, this elastic analysis gives the qualitative stress distribution rather than the actual stress distribution in the slab. Singularity in the solution exists right at the position of maximum stress, along the length of the stud. Thus the exact load at failure cannot be predicted from the above elastic analysis.

3.2 ULTIMATE STRENGTH ANALYSIS AT INCIPIENT FAILURE

3.2.1 Redistribution of loading after the tensile crack. After development of the tensile crack, stresses in the slab are redistributed. The slab may then be treated as a quarter plane with the load applied along part of one boundary by the studs, Fig. 14. An unsuccessful attempt was made to find the plane stress elasticity solution for this problem. It was then decided that an ultimate strength analysis at incipient failure would be more successful.

3.2.2 Assumption and analysis. Experimental observations of the narrow slab indicate that the final failure was caused by shearing along surface AB, Fig. 15. I. Evans (7) successfully applied an ultimate strength analysis in the breakage of coal. However, it was necessary to modify Evan's analysis considerably because in the case of coal a splitting wedge was used to produce a maximum principal stress failure.

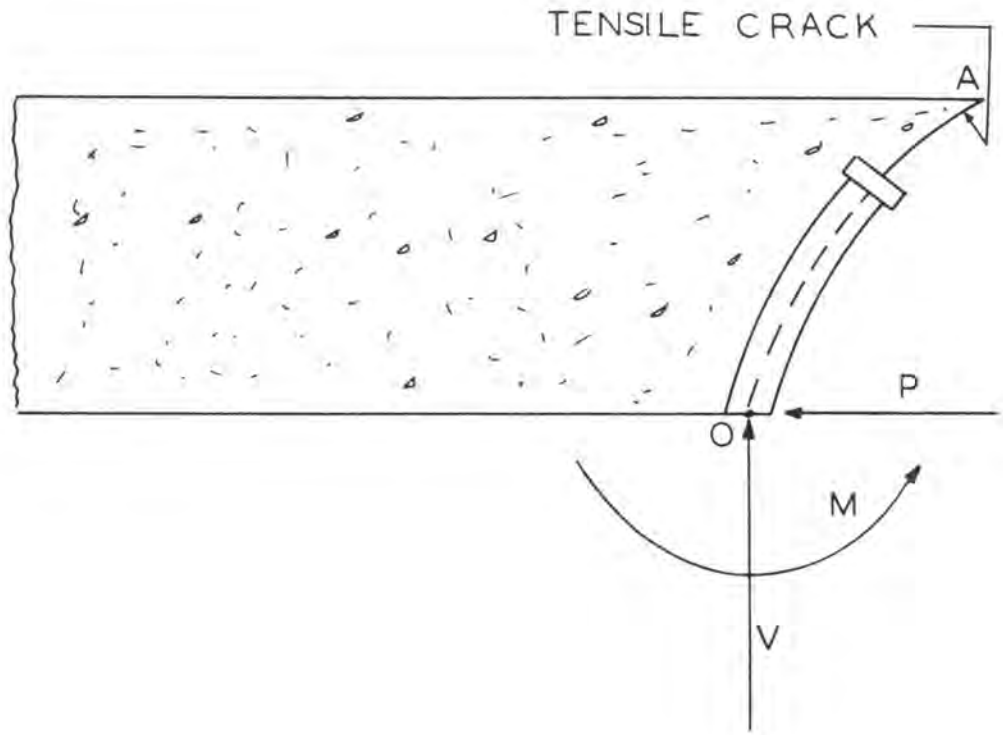

FIG.14 REDISTRIBUTION OF LOADING AFTER THE TENSILE CRACK

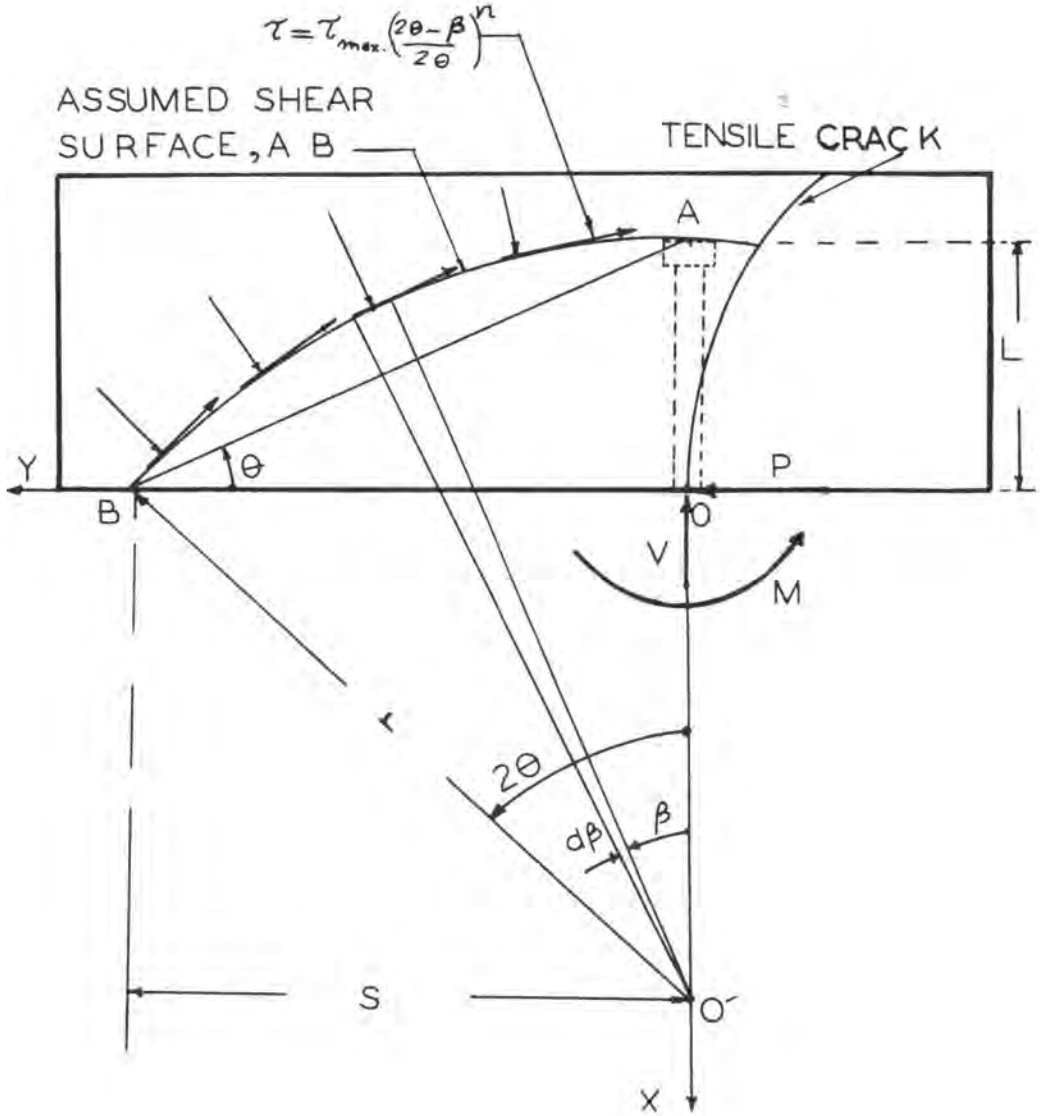

FIG.15 ASSUMED FAILURE SURFACE, AB

In our problem, the shear failure proceeds essentially by propagation of the shear crack, starting from A and finally reaching the free surface at B, Fig. 15. The shear surface AB, is assumed to be a circular arc with the center of the circle O', lying on the OX axis. The variation of shear stress at incipient failure is assumed to be according to the power law, $\tau = \tau_{max.}\left(\frac{2\theta-\beta}{2\theta}\right)^n$ where, θ and β are angles as shown in Fig. 15, n is an empirically determined exponent, and $\tau_{max.}$ is the shear strength of the concrete.

From Fig. 15,

$$\frac{L}{s} = \tan\theta$$

therefore, the failure length,

$$s = \frac{L}{\tan\theta} \tag{11}$$

where L = stud length

Also, $$\frac{s}{r} = \sin 2\theta \tag{12}$$

From Eq. (11) and Eq. (12)

$$r = \frac{L}{2\sin^2\theta} \tag{13}$$

Taking moments about O', Fig. 15,

$$P(r-L) + M = \int_0^{2\theta} \tau_{max.}\left(\frac{2\theta-\beta}{2\theta}\right)^n \cdot w \cdot r^2 \cdot d\beta$$

$$= \frac{\tau_{max.} w \cdot r^2}{n+1} \cdot 2\theta \tag{14}$$

where, w = width of the slab

P = ultimate load

For practical configurations of stud shear connectors, the plastic moment capacity of the studs, M is only 1 to 2 percent of the total moment and hence can be omitted for simplicity of the calculation. Then,

$$P = \frac{\tau_{max.} w \cdot r^2}{n+1} \cdot \frac{2\theta}{(r-L)} \tag{15}$$

From Eq. (13) and Eq. (15),

$$P = \frac{\tau_{max.} w \cdot L}{n+1} \frac{\theta}{\sin^2\theta \cos 2\theta} \tag{16}$$

If P is now minimized with respect to θ, then from the necessary condition of minima, $\frac{\partial P}{\partial \theta} = 0$,

$$1 + 2\theta(\tan 2\theta - \cot\theta) = 0 \tag{17}$$

The above transcendental equation 17, was solved graphically and the angle θ found to be 0.41 radians. With θ equal to 0.41 radians, Eq. 16 was checked for the sufficiency condition of minima, $\frac{\partial^2 P}{\partial \theta^2} > 0$. The experimental values of θ for the narrow rectangular pushout specimens varied from 0.39 radians to 0.43 radians, Table II.

The direct shear strength of concrete, $\tau_{max.}$, according to H. J. Cowan (8) is approximately equal to $f'_c/4$.

Thus,

$$\tau_{max.} \cong f'_c/4 \tag{18}$$

From Eq. 16,

$$n = \frac{\tau_{max.} w \cdot L}{P} \quad \frac{\theta}{\sin^2\theta \cos 2\theta} - 1 \tag{19}$$

With the theoretical value of θ equal to 0.41 radians, the value of n for each of the the test specimens was calculated from Eq. (19) using the experimental values of P, Table II. It appeared that a value of n equal to 5 would thus serve to bring the theory very close into line with the experimental observations.

3.2.3 Comparison of Experiment and Theory. Using n equal 5, the theoretical values of P for the pushout specimens were calculated from Eq. 16. The load per connector Q, is P/N, where N is

TABLE II

VALUES OF θ AND n

Specimen	L (inches)	D (inches)	w (inches)	f'_c (ksi)	$\tau_{max.}$ (ksi)	Expt. P (kips)	Expt.θ (radians)	Theo.θ (radians)	Calculated n
N6B4HS-1	4.0	.750	8.0	8.28	2.07	37.0	0.39	0.41	5.72
N6B4HS-2	4.0	.750	8.0	8.28	2.07	47.5	0.43	0.41	4.25
N6B4HS-3	4.0	.750	8.0	6.861	1.715	34.25	0.42	0.41	5.03
N6B4HS-4	4.0	.750	8.0	6.861	1.715	40.0	0.42	0.41	4.17

the total number of studs at section AO, Fig. 15. Comparison between the theoretical and the experimental values of Q is shown in Table III.

The strength of each of the haunched sections tested by Sweeney (4) and Buttry (5) was compared with the theory by computing the strength of shear connectors in a narrow rectangular slab with a width equal to the average width, $w_{av.}$, of the haunch, Fig. 16. The hypothesis of course is that the strengths of connectors in this rectangular slab would be less than that of the connectors in the haunched section. The theoretical results seem to agree very well with the experimental observations, Tables IV and V.

3.2.4 Analysis of the load per shear connection with more than one line of studs in the zone of influence. When there is more than one line of studs in the zone of influence O_1A_1B, Fig. 17, it was assumed that $\hat{P}_1$, V_1 and M_1 at O_1 were resisted by the stresses on failure surface A_1B_1. Similarly $\hat{P}_2$, V_2 and M_2 at O_2 and $\hat{P}_3$, V_3 and M_3 at O_3 were assumed to be resisted by the stresses on failure surfaces A_2B_2 and A_3B_3 respectively. The surfaces A_1B_1, A_2B_2 and A_3B_3 were assumed to be the circular arcs with centers at O_1', O_2' and O_3' respectively. For the uniform stud spacing, $\hat{s}$, and also for the same size and number of studs at each section O_1A_1, O_2A_2 and O_3A_3, the components of forces at O_1 are equal to that of the forces at O_2 and O_3 and thus can be denoted by the symbols, $\hat{P}$, V and M only.

From these assumptions, the strength of each shear connection, $\hat{P}$, may be expressed as a function of the stud spacing, $\hat{s}$,

TABLE III

COMPARISON OF THEORETICAL LOAD PER CONNECTOR
WITH EXPT. RESULTS FROM PUSHOUT TESTS

Specimen	D (inches)	L (inches)	w (inches)	f'_c (ksi)	$\tau_{max.}$ (ksi)	Expt. Q (kips)	Theo. Q (Eq. 16) (kips)	Failure
N6B4HS-1	.750	4.0	8.0	8.28	2.07	18.5	20.8	Concrete
N6B4HS-2	.750	4.0	8.0	8.28	2.07	23.75	20.8	Concrete
N6B4HS-3	.750	4.0	8.0	6.86	1.715	17.12	17.2	Concrete
N6B4HS-4	.750	4.0	8.0	6.86	1.715	20.0	17.2	Concrete

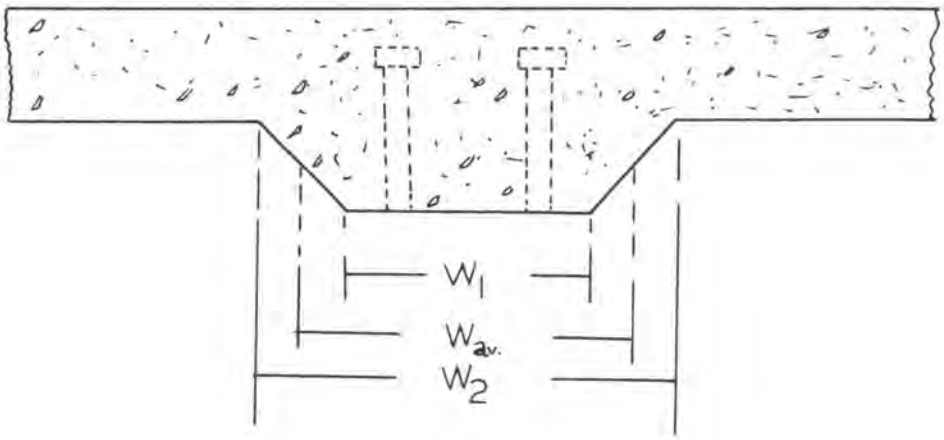

NOTE :

AVERAGE WIDTH OF THE HAUNCH, $W_{av.} = \frac{W_1 + W_2}{2}$

FIG.16 HAUNCHED SECTION

TABLE IV*

COMPARISON OF THEORETICAL LOAD PER CONNECTOR
WITH EXPT. RESULTS OF THE HAUNCHED SECTIONS
TAKEN FROM BUTTRY'S WORK (2)

Specimen	D (inches)	L (inches)	$w_{av.}$ (inches)	f'_c (ksi)	$\tau_{max.}$ (ksi)	Expt. Q[1] (kips)	Theo. Q[2] (kips)	Failure
N5H4B2.5	5/8	2.5	14	4.56	1.14	14.6	12.5	Pull out
L5H4A2.5	5/8	2.5	14	3.44	0.86	11.7	9.5	Pull out
N6H4A4	3/4	4	14	4.19	1.05	20.8	18.4	Concrete
N6H4B4	3/4	4	11	4.54	1.13	22.5	15.7	Concrete
L6H4A4	3/4	4	14	3.92	0.98	15.6	17.2	Concrete
L6H4B4	3/4	4	11	4.19	1.05	17.5	14.5	Concrete

[1] for the haunched section

[2] for the equivalent narrow rectangular section

* the value of Q for connectors in a narrow rectangular slab is a lower bound for the value of Q for connectors in the haunched section

TABLE V*

COMPARISON OF THEORETICAL LOAD PER CONNECTOR
WITH EXPT. RESULTS OF THE HAUNCHED SECTION
TAKEN FROM SWEENEY'S WORK (1)

Specimen	D (inches)	L (inches)	$W_{av.}$ (inches)	f'_c (ksi)	$\tau_{max.}$ (ksi)	Expt. Q[1] (kips)	Theo. Q[2] (kips)	Failure
LFB7-1	7/8	4	8.5	6.13	1.53	20.5	15.9	Concrete

[1] for the haunched section

[2] for the equivalent narrow rectangular section

* the value of Q for connectors in a narrow rectangular slab is a lower bound for the value of Q for connectors in the haunched section

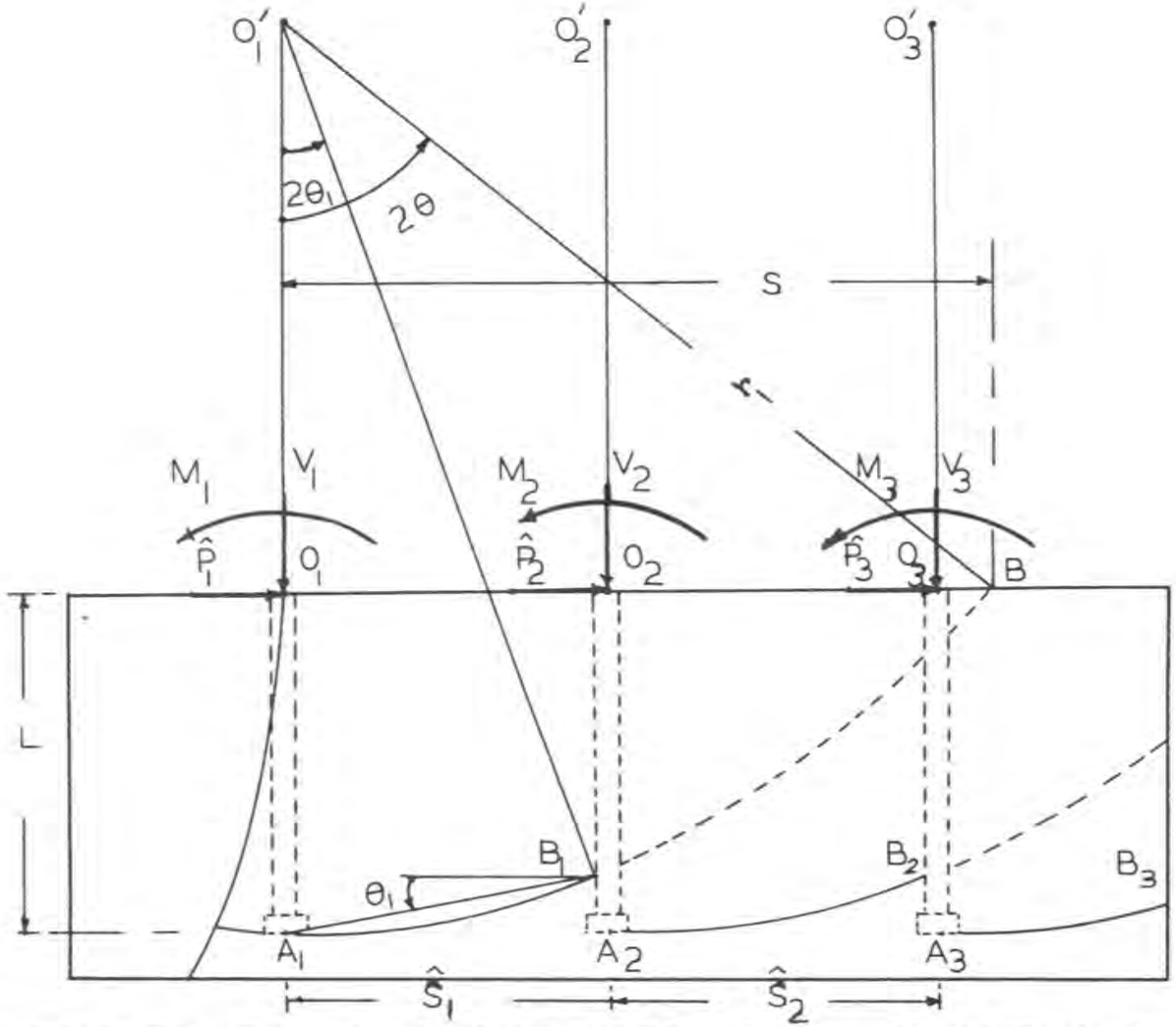

FIG.17 ASSUMED FAILURE SURFACES, A_1B_1, A_2B_2 AND A_3B_3

as follows:

From Fig. 17,

$$\hat{s}_1 = r_1 \sin 2\theta_1 \tag{20}$$

For the uniform stud spacing, the above equation becomes,

$$\hat{s} = r \sin 2\theta_1 \tag{21}$$

From Eq. (13) and Eq. (21),

$$\theta_1 = \tfrac{1}{2}\sin^{-1}\left(\frac{2\hat{s}\ \sin^2\theta}{L}\right) \tag{22}$$

Taking moments about O_1', Fig. 17,

$$\hat{P}_1(r-L) + M_1 = \int_0^{2\theta_1} \tau_{max.} \left(\frac{2\theta-\beta}{2\theta}\right)^n w \cdot r^2 d\beta \tag{23}$$

Again the plastic moment, M_1, in the studs at the section O_1A_1 is small and may be neglected. Therefore from Eq. (23),

$$\hat{P}_1 = \frac{\tau_{max.} w \cdot L}{n+1} \ \frac{\theta}{\sin^2\theta \cos 2\theta} \cdot \left[1-\left(\frac{\theta-\theta_1}{\theta}\right)^{n+1}\right] \tag{24}$$

Thus for the uniform stud spacing, $\hat{s}$, we can write

$$\hat{P} = \frac{\tau_{max.} w \cdot L}{n+1} \ \frac{\theta}{\sin^2\theta \cos 2\theta} \left[1-\left(\frac{\theta-\theta_1}{\theta}\right)^{n+1}\right] \tag{25}$$

where,

$$\tau_{max.} = \frac{f_c'}{4}$$

$$n = 5$$

$$\theta = .41 \text{ radians}$$

$$L = \text{stud length}$$

$$w = \text{width of the slab}$$

and, $$\theta_1 = \tfrac{1}{2}\sin^{-1}\left(\frac{2\hat{s}\ \sin^2\theta}{L}\right)$$

As the spacing of the studs, $\hat{s}$, approaches the failure length, s, Fig. 17, the load $\hat{P}$ approaches the value of P as computed from Eq. 16.

As $\hat{s}$ approaches zero the failure surface approaches a horizontal plane with a uniform shear stress of $\tau_{max.}$. Thus for

very small values of $\hat{s}$,

$$\hat{P} = \hat{s} \cdot w \cdot \tau_{max}. \tag{26}$$

A dimensionless plot relating $\hat{P}$ and $\hat{s}$ is presented in Chapter IV.

CHAPTER IV

DESIGN IMPLICATIONS

4.1 INTRODUCTION

The analysis developed in Chapter III is for shear connectors in narrow rectangular slabs. This analysis can be used to estimate the strength of shear connectors in haunched sections provided reasonable judgment is used in choosing a width for an equivalent rectangular section.

In cases where the shear connectors project only a short distance into the haunch, the strength of the shear connection may be estimated with a fair degree of accuracy by considering a narrow rectangular slab with a width equal to the minimum width of the haunch. In cases where the shear connectors are nearly as long as the depth of the haunch, the average haunch width may be used. Computations based on average haunch width become more conservative when the stud length exceeds the haunch depth.

The strength of shear connectors in the haunched sections tested by Sweeney (4) and Buttry (5) was compared with the strength of shear connectors in a narrow rectangular slab with a width equal to the average width, $w_{av.}$, of the haunch. The theoretical results agreed very well with the experimental observations, Tables IV and V.

4.2 RELATIONSHIP BETWEEN THE WIDTH OF THE SLAB AND THE TOTAL FORCE AT THE SECTION OF SHEAR CONNECTORS

A family of curves showing the relationship between the width of the slab, w, and the shear connection strength, P, for various stud lengths, L, is shown in Fig. 18. These curves are based on Eq. (16) and a compressive strength of concrete, f'_c, equal to 4,000 psi.

From Eq. (16),

$$P = \frac{\tau_{max.} \; w \cdot L}{n+1} \quad \frac{\theta}{\sin^2\theta \cos 2\theta}$$

where, P = shear connection strength

$\tau_{max.} = f'_c/4$

$n = 5$

w = width of the slab

L = stud length

θ = 0.41 radians

The force per connector, Q, equals P/N, where N is the total number of studs at the section of the shear connection.

According to Buttry (5), the ultimate shearing strength of a stud in a solid slab is:

$$Q_s = \pi/4 \cdot D^2 \cdot f'_s \tag{27}$$

where, D = diameter of the studs

f'_s = shearing strength of steel

It is clear that the strength of any shear connection may not exceed the sum of the strengths of the shear connectors in that connection. Limiting values for pairs of various sizes of studs are shown in Fig. 18 as dashed lines.

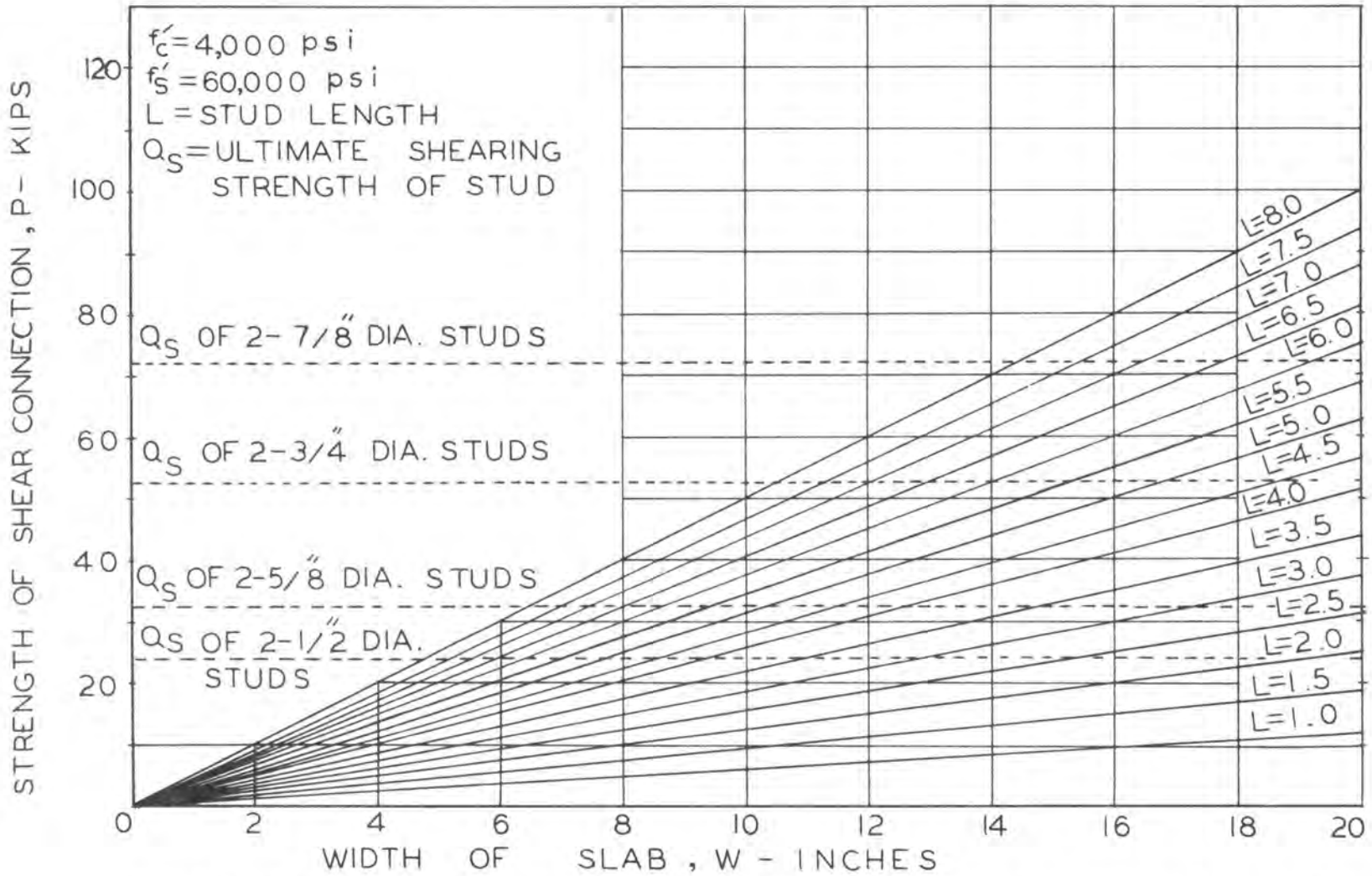

FIG.18 STRENGTH OF SHEAR CONNECTION VS. WIDTH OF SLAB

4.3 RELATIONSHIP BETWEEN THE SPACING OF STUDS AND THE STRENGTH OF THE SHEAR CONNECTION

A dimensionless relationship between the strength of the shear connection, $\hat{P}$, and the spacing of shear connectors, $\hat{s}$, can be established from the previous chapter.

From Eq. (11), the failure length, Fig. 15,

$$s = L/\tan\theta$$

Equations (16), (22) and (25) may be combined to form the dimensionless relationship,

$$\hat{P}/P = 1 - \left(\frac{\theta-\theta_1}{\theta}\right)^{n+1} \tag{28}$$

where, $n = 5$

$$\theta_1 = \tfrac{1}{2}\sin^{-1}(\sin 2\theta \cdot \hat{s}/s) \tag{29}$$

$\theta = 0.41$ radians

$\hat{s}$ = stud spacing

and s = failure length, Fig. 15.

A dimensionless plot described by Eqs. (28) and (29) is shown as curve AB in Fig. 19. As $\hat{s}$ approaches the value of s, $\hat{P}/P$ approaches unity, represented by point A in Fig. 19.

For very close stud spacing $\hat{s}$, the strength of the connection is limited by the shear strength of a horizontal plane through the slab. This limiting value may be expressed as,

$$\hat{P} = \tau_{max.} \cdot \hat{s} \cdot w \tag{30}$$

Therefore the dimensionless relationship for close spacings is as follows:

$$\hat{P}/P = 3/2 \;\; \hat{s}/s \;\; \sin 4\theta/\theta \tag{31}$$

The plot of Eq. (31) is shown by the straight line OB in Fig. 19.

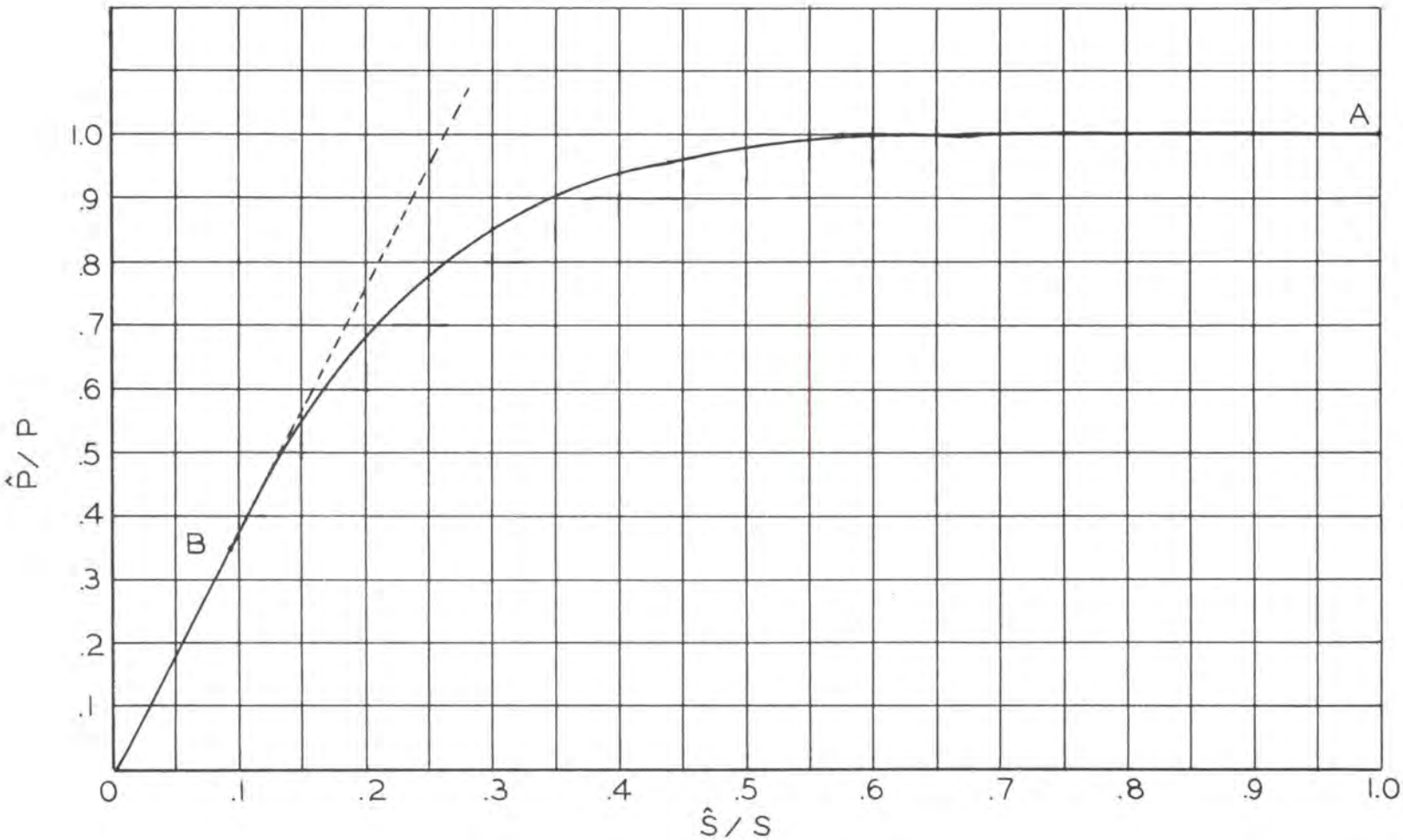

FIG. 19 DIMENSIONLESS PLOT OF SHEAR CONNECTION STRENGTH VS. STUD SPACING

Thus the curve ABO can be effectively used to determine the load per shear connection, $\hat{P}$, for various stud spacings.

CHAPTER V

CONCLUSIONS

The following conclusions were drawn from the present work.

1. Since material nonlinearity exists in concrete even at low stress, the plane stress elastic solution gives the qualitative stress distribution rather than the actual distribution of stress in slabs. Singularity in the solution exists right at the position of maximum stress and thus the exact load at failure cannot be predicted from the elastic analysis.

2. The ultimate strength analysis at incipient failure developed for shear connections in narrow rectangular slabs can be used to estimate the strength of shear connections in haunched sections provided a reasonable judgment is used in choosing a width for an equivalent rectangular section. In cases where the shear connectors project only a short distance into the haunch, the strength of the shear connection may be estimated with a fair degree of accuracy by considering a narrow rectangular slab with a width equal to the minimum width of the haunch. In cases where shear connectors are nearly as long as the depth of the haunch, the average haunch width may be used. Computations based on average haunch width become more conservative when the stud length exceeds the haunch depth.

3. For a single line of studs in the zone of influence, the total force at the section of shear connection is given by,

$$P = \frac{\tau_{max.} \cdot w \cdot L}{n+1} \frac{\theta}{\sin^2\theta \cos 2\theta}$$

where,

$\tau_{max.} \cong f'_c/4$

w = width of the slab

L = stud length

n = 5

θ = 0.41 radians

Thus the force per connector, Q, is equal to P/N, where N is the number of studs at the section of shear connection.

4. For more than a single line of studs in the zone of influence the relationship between the spacing of studs, $\hat{s}$, and the total force, $\hat{P}$, at the section of shear connection is given by,

$$\hat{P} = \frac{\tau_{max.} \cdot w \cdot L}{n+1} \frac{\theta}{\sin^2\theta \cos 2\theta} \cdot \left[1-\left(\frac{\theta-\theta_1}{\theta}\right)^{n+1}\right]$$

where,

$$\theta_1 = \tfrac{1}{2}\sin^{-1}\left(2\hat{s}\frac{\sin^2\theta}{L}\right)$$

and the force per connector, $\hat{Q}$, is equal to $\hat{P}/N$.

SELECTED REFERENCES

1. Caughey, R. A., "Composite Beams of Concrete and Structural Steel," Proc. 41st Annual Meeting, Iowa Engineering Society, pp. 96-104, 1929.

2. "Standard Specifications for Highway Bridges," The American Association of State Highway Officials, 4th Edition, 1944.

3. "Standard Specification for Highway Bridges," The American Association of State Highway Officials, 7th Edition, 1957.

4. Sweeney, G. M., "Load-Deformation Behavior of Composite Bridge Stringers," Master's Thesis, Dept. of Civil Engineering, University of Missouri, February, 1965.

5. Buttry, K. E., "Behavior of Stud Shear Connectors in Lightweight and Normal Weight Concrete," Master's Thesis, Dept. of Civil Engineering, University of Missouri, August, 1965.

6. Melan, E., "Der Spannungszust der durch eine Einzelkraft in Inner beamsprechten Halbscheibe," Journal of The Zeitchrift fur Angewandte Mathematik and Mechanik, Vol. 12, 1932, pp. 343 and Vol. 20, 1940, pp. 368.

7. Evans, I., "Theoretical Aspects of Coal Ploughing," Proceedings of a Conference on Non-Metallic Brittle Materials, London 1958, pp. 451.

8. Cowan, H. J., "The Strength of Plain, Reinforced and Prestressed Concrete Under the Action of Combined Stresses, with Particular Reference to the Combined Bending and Torsion of Rectangular Sections," Magazine of Concrete Research, Number 13, August 1953, pp. 75.

MoDOT Library
RD0016327